J. Fluid Mech. (1991), *vol.* 225, *pp.* 81–100
Printed in Great Britain

Square patterns and secondary instabilities in driven capillary waves

By S. T. MILNER
AT&T Bell Laboratories, Murray Hill, NJ 07974, USA

(Received 19 January 1990 and in revised form 9 July 1990)

Amplitude equations (including nonlinear damping terms) are derived which describe the evolution of patterns in large-aspect-ratio driven capillary wave experiments. For drive strength just above threshold, a reduction of the number of marginal modes (from travelling capillary waves to standing waves) leads to simpler amplitude equations, which have a Lyapunov functional. This functional determines the wavenumber and symmetry (square) of the most stable uniform state. The original amplitude equations, however, have a secondary instability to transverse amplitude modulation (TAM), which is not present in the standing-wave equations. The TAM instability announces the restoration of the full set of marginal modes.

1. Introduction

The aim of this work is to give a systematic account of the formation of regular patterns and their secondary instabilities in parametrically driven capillary wave systems of large aspect ratio. The parametric instability of a fluid–air interface driven by vertical oscillations was first observed and investigated by Faraday (1831) and is associated with his name.

In cells sufficiently large and deep compared to the resonant wavelength of the pattern, and with a sufficiently clean free surface, the many complex processes of damping at the walls (Miles 1967), meniscus (Cox 1986; Hocking 1987), and surface layer (Miles 1967) of the cell may be neglected. A large enough system also allows the effects of the finite cell size on pattern selection (Douady & Fauve 1988) to be neglected. The present work explores mechanisms of pattern selection and secondary instability which depend on nonlinear interactions between modes in an infinite system.

While many experiments on driven surface waves have been performed on small cells, i.e. on parametric resonance of low-order modes (Douady & Fauve 1988; Ciliberto & Gollub 1985; Simonelli & Gollub 1989), some experiments have also been performed (Ezerskii, Korotin & Rabinovich 1985; Ezerskii *et al.* 1986; Levin & Trubnikov 1986; Tufillaro, Ramshankar & Gollub 1989) in which the cell is on the order of 100 wavelengths on a side. These latter experiments display several remarkable features, including (i) square patterns, even in cylindrical containers; (ii) a secondary instability to a pattern with transverse modulations of the amplitude of standing waves, but with long-range order retained; (iii) at still higher drive strength, a transition to spatiotemporal chaos.

Estimates of how big a cell is required for neglect of boundary effects to be a good approximation may be given in terms of the various lengths in the problem, i.e. the system size L, the viscous penetration depth l, and the wavelength λ. These estimates

are satisfied by experiments similar to those of Ezerskii *et al.* (1986) and Tufillaro *et al.* (1989); the requirements are derived, following Miles (1967) and Cox (1986) in Appendix C.

Additionally, large-aspect-ratio cells provide an essentially continuous spectrum of modes in which the system may respond to the drive; complications resulting from a discrete spectrum are absent. (The more subtle effects of boundary conditions on wavenumber selection described in Cross *et al.* (1983) may in principle be present in large-aspect-ratio capillary wave cells, but we will not consider this possibility here.)

In the absence of boundary effects, nonlinear interactions in the bulk of the cell between growing capillary waves will determine the symmetry and wavelength of regular patterns, much as the preference for rolls of a given width in Rayleigh–Bénard cells is determined by interactions between incipient rolls in the bulk of the cell. In §2, we employ the methods of Newell & Whitehead (1969) to obtain amplitude equations for the neutral modes of the system in the absence of damping, which are travelling capillary waves with frequency ω equal to the subharmonic of the drive frequency 2ω. Ezerskii *et al.* (1986) first derived equations of this form (but with linear damping terms only, and coefficients which differ from the results of the present work) under the assumption of a square pattern (which is observed experimentally). To understand the origin of the square pattern, we derive evolution equations for patterns of general symmetry. Readers who are not concerned with the method of derivation may skip to the discussion immediately preceding equations (14)–(16).

We derive linear and nonlinear damping terms for the amplitudes of the travelling waves in §3. It turns out to be essential to consider nonlinear damping as a mechanism stabilizing the amplitude of regular patterns, in the physical situation that the system (rather than the experimenter) selects the wavelength of the pattern. Any non-dissipative mechanism for shifting the frequency of a growing mode at finite amplitude may be totally compensated by the system choosing a mode sufficiently off resonance; this leads in the absence of nonlinear damping terms to unbounded amplitudes at any value of drive above threshold, if the system is free to adjust the wavenumber globally. (It is possible that for some set of boundary conditions, global adjustment of the wavenumber is suppressed or eliminated. The intent of this paper is to investigate what happens if this is not so. Much of the paper, i.e. the derivation of the amplitude equations with damping for arbitrary angles between waves (§§2 and 3), does not depend on this assumption.)

The set of amplitude equations for the travelling capillary waves, including the non-linear damping terms, is neither Hamiltonian, nor derivable from a Lyapunov functional. However, for drive strengths sufficiently close to threshold (determined by the damping strength, which is assumed to be small), the damping splits the degeneracy between the growth rates of two standing capillary waves (both of which are neutral modes at zero drive in the absence of damping). This results in two standing waves of different growth rates, and a non-zero drive threshold for the faster-growing standing wave. Thus for drive strength close to threshold, the number of neutral modes is reduced by half. Riecke (1990) in a recent paper obtained (for the one-dimensional case) new, simpler amplitude equations by assuming essentially that the amplitude of the decaying standing wave is determined adiabatically by the growing standing wave. We construct these equations, for the present case of arbitrary patterns in two dimensions, in §4. These simpler amplitude equations are (with some restrictions) derivable from a Lyapunov functional. Thus, the symmetry and wavenumber of the most stable pattern may be found from minimizing the

appropriate Lyapunov functional. Using our results for the nonlinear couplings for patterns of general symmetry, we find that square patterns indeed give the deepest minimum in the functional of the usual high-symmetry candidates (single waves, square and hexagonal patterns).

In §5 we investigate the secondary instabilities of the uniform square pattern. The simplified amplitude equation has both transverse (zigzag) and longitudinal (Eckhaus) instabilities (Eckhaus 1965; Newell & Whitehead 1969) of the usual sort; however, the path of the most stable state through the drive-wavenumber plane never intersects an Eckhaus boundary. Instead, it turns out that the full amplitude equations, which contain the dynamics of the decaying standing waves neglected in the adiabatic approximation, display an instability of the uniform pattern to transverse amplitude modulations (TAM) (Ezerskii *et al.* 1986) which is not present in the simpler amplitude equations. Clearly, the small splitting between the two standing waves induced by weak damping does not continue to be important for increasingly strong drive. The TAM instability explicitly depends on and indeed may be said to announce the failure of the adiabatic approximation, and the return to relevance of the neglected modes. We show that the path of the most stable uniform state collides with the TAM instability boundary.

Finally, in the concluding Section we make quantitative comparisons between the present theory and the experiments of Tufillaro *et al.* (1989) which appear to satisfy the large-system requirements for validity of our theory. We find semi-quantitative agreement in the value of threshold drive strength, as well as for the pattern amplitude, unstable wavenumber, and drive strength at the TAM instability. The predictions for quantities at the TAM instability, particularly the drive strength, are rather sensitive to the values of the nonlinear couplings. Errors by a factor of three due to neglect of higher-order terms in our expansions, or boundary effects, such as damping within the viscous penetration depth at the free surface due to surface contamination, would be sufficient to achieve quantitative agreement.

2. Amplitude equations

Our starting point for deriving amplitude equations for the Faraday instability is the set of ideal-fluid equations (Benjamin & Ursell 1954) for the velocity potential $\phi(x, y, z)$,

$$\dot{\phi} + \tfrac{1}{2}(\nabla\phi)^2 + p + fz\cos 2\omega t = 0, \tag{1}$$

with the incompressibility condition

$$\nabla^2\phi = 0, \tag{2}$$

and the convective equation of motion for the height $\zeta(x, y)$ of the free surface

$$\dot{\zeta} + \nabla\phi\cdot\nabla\zeta = \hat{z}\cdot\nabla\phi. \tag{3}$$

The constitutive equation for the pressure due to surface tension is given by $p = \Sigma(c_1 + c_2)$, where c_1 and c_2 are the principal radii of curvature, which leads to

$$p = -\Sigma\nabla\cdot[\nabla\zeta/(1+(\nabla\zeta)^2)^{\frac{1}{2}}]. \tag{4}$$

The equation for the Laplace pressure is meant to be evaluated at the free surface, of course, so that is the most convenient place to enforce the Bernoulli equation. However, it is inconvenient to evaluate ϕ on the surface (as is also required for

computing the motion of the surface); instead, we expand ϕ on the surface in terms of ϕ at $x = 0$:

$$\phi(x, y, \zeta(x, y)) = \phi(x, y, 0) + \zeta(x, y) \left.\frac{\partial \phi(x, y, z)}{\partial z}\right|_{z=0} + \tfrac{1}{2}\zeta^2 \frac{\partial^2 \phi}{\partial z^2} \ldots, \tag{5}$$

and similarly for space and time derivatives of ϕ.

We also expand the pressure to $O(\zeta^3)$; then the Bernoulli and surface-convection equations may be written

$$\dot{\phi} - \Sigma \nabla^2 \zeta + f\zeta \cos 2\omega t + N_\phi(\phi, \zeta) = 0, \tag{6}$$

$$\dot{\zeta} - \frac{\partial \phi}{\partial z} + N_\zeta(\phi, \zeta) = 0, \tag{7}$$

with the nonlinear terms expanded to third order in the fields as

$$N_\zeta = \zeta \nabla_\perp^2 \phi + \tfrac{1}{2}\zeta^2 \partial_z \nabla_\perp^2 \phi + \nabla_\perp \phi \cdot \nabla \zeta + \zeta \nabla \zeta \partial_z \cdot \nabla_\perp \phi, \tag{8}$$

$$N_\phi = \tfrac{1}{2}\Sigma \nabla^2 \zeta (\nabla \zeta)^2 + \tfrac{1}{2}\Sigma \nabla \zeta \cdot \nabla (\nabla \zeta)^2 + \zeta \partial_z \dot{\phi} - \tfrac{1}{2}\zeta^2 \nabla_\perp^2 \dot{\phi} + \tfrac{1}{2}(\nabla \phi)^2 + \tfrac{1}{2}\zeta \partial_z (\nabla \phi)^2. \tag{9}$$

We follow the procedure of Newell & Whitehead (1969) to derive amplitude equations for the above hydrodynamics. The marginally growing or neutral solutions are the solutions of the linearized equations. In the present case, these are the set of travelling capillary waves, with any wavevector. Because we are driving the system parametrically (Landau & Lifshitz 1976) at frequency 2ω, we expect the response to be at ω. Hence we take as the lowest-order solutions a sum over capillary waves at frequency ω with some set $\{\boldsymbol{k}_j\}$ of wavevectors:

$$\zeta_0 = \sum_j a_j(X, T) \exp(\mathrm{i}\boldsymbol{k}_j \cdot \boldsymbol{x} - \mathrm{i}\omega t) + \text{c.c.}, \tag{10}$$

$$\phi_0 = \frac{-\mathrm{i}\omega}{k} \exp(kz) \sum_j a_j(X, T) \exp(\mathrm{i}\boldsymbol{k}_j \cdot \boldsymbol{x} - \mathrm{i}\omega t) + \text{c.c.} \tag{11}$$

Here $k = |\boldsymbol{k}_j|$ and $\boldsymbol{k}_{-j} = -\boldsymbol{k}_j$, the variables x and X are two-dimensional, and the variables X and T are slowly varying.

An expansion bookkeeping parameter ϵ is introduced, with $X = \epsilon x$, $T = \epsilon t$, $\nabla \to \nabla + \epsilon \nabla_X$, $\partial_t \to \partial_t + \epsilon \partial_T$. Here $\nabla = \nabla_x + \hat{z}\partial_z$, and ∇_x and ∇_X are gradients in the plane. Note that the z-dependence of the fields is not slow, since the flow decays into the fluid on a lengthscale k^{-1}; hence there is no '∂_Z'.

The fields are expanded as $\zeta = \epsilon\zeta_0 + \epsilon^2\zeta_1 + \epsilon^3\zeta_2 + \ldots$, the drive as $f = \epsilon f_0 + \epsilon^2 f_1 + \ldots$. The linear operator of (6) and (7) is expanded as $L = L_0 + \epsilon L_1 + \epsilon^2 L_2 + \ldots$, and the nonlinear parts as e.g., $N_\zeta = \epsilon^2 N_\zeta^{(1)} + \epsilon^3 N_\zeta^{(2)} + \ldots$.

Equations (6) and (7) may then be expanded in powers of ϵ to give

$$\left.\begin{aligned} L_0 \Psi_0 &= 0, \\ L_0 \Psi_1 + L_1 \Psi_0 + N_1 &= 0, \\ L_0 \Psi_2 + L_1 \Psi_1 + L_2 \Psi_0 + N_2 &= 0, \end{aligned}\right\} \tag{12}$$

where $\Psi \equiv (\zeta, \phi)$ and $N \equiv (N_\zeta, N_\phi)$. The first equation gives the neutral solutions. The second equation has a solvability condition, which determines the group velocity in the equation of motion for the $\{a_j\}$; when this condition is enforced, the second equation gives the second-harmonic response of Ψ. The solvability condition for the third equation gives further terms linear in gradients of a_j, which shift the frequency

of the capillary waves along the dispersion relation; in addition, the second harmonics mix with the neutral modes to give a resonant three-wave response, which gives cubic terms in the equation of motion for the $\{a_j\}$.

The incompressibility condition $\nabla^2\phi = 0$ must be enforced order by order in ϵ as well. The expansion generates the equations

$$\left.\begin{aligned} \nabla^2\phi_0 &= 0, \\ \nabla^2\phi_1 + 2\nabla\cdot\nabla_X\phi_0 &= 0, \\ \nabla^2\phi_2 + 2\nabla\cdot\nabla_X\phi_1 + \nabla_X^2\phi_0 &= 0. \end{aligned}\right\} \tag{13}$$

These may be solved order by order, by finding particular solutions $\phi_i^{(\mathrm{p})}$ which satisfy the ith incompressibility equation, and then writing the ith non-resonant correction as $\phi_i = \phi_i^{(\mathrm{h})} + \phi_i^{(\mathrm{p})}$, where $\nabla^2\phi^{(\mathrm{h})} = 0$. The solvability condition will be affected by $\phi^{(\mathrm{p})}$, but the non-resonant correction $\phi^{(\mathrm{h})}$ extracted at $z = 0$ from the ith equation of motion may trivially be extended to give $\nabla^2\phi_i^{(\mathrm{h})} = 0$ (and hence no effect on the ith incompressibility equation) by multiplying by $\exp(qz)$ with the appropriate q.

Some details of the expansion are given in Appendix A. The following aspects of the procedure are worth noting:

(i) The form of the nonlinear terms in the equation of motion for a_j up to cubic order must be $\mathrm{i}T_{jk}^{(1)}|a_k|^2 a_j + \mathrm{i}T_{jk}^{(2)} a_k a_{-k} a_{-j}^*$, with $T_{jk}^{(1)}$ and $T_{jk}^{(2)}$ real as we have not yet included damping. The reason is that the capillary waves that these amplitudes multiply must have frequencies and wavevectors which sum to the frequency and wavevector of the wave corresponding to a_j, i.e. the terms must be resonant. Because of the requirement that the frequencies of the waves sum to ω, there can be no terms of even order in the $\{a_j\}$. This absence of, for example, quadratic terms suggests that hexagonal patterns will not be favoured.

(Our expansion to third order in ϵ neglects terms studied by Zakharov, L'vov & Starobinets (1971) of the form $f a_k^* a_{-k}^* a_j$, which gives an amplitude dependence to the drive coupling and a mechanism for limiting pattern amplitudes different from those of the present work. These terms are $O(\epsilon^4)$ and are negligible here.)

(ii) The form of the linear gradient terms in the equation for $\dot{a}_j$ is prescribed by the dispersion relation. That is, $a_j(x,t) = \exp(\mathrm{i}\Delta\boldsymbol{k}\cdot\boldsymbol{x} - \mathrm{i}\Delta\omega(\Delta k)\,t)$ should be a solution of the equations of motion. The dispersion relation $\omega^2 = \Sigma k^3$ implies an expansion of the form

$$\Delta\omega = \frac{\partial\omega}{\partial k}\left((\hat{\boldsymbol{k}}\cdot\Delta\boldsymbol{k}) + \frac{(\Delta\boldsymbol{k})^2}{2k} - \frac{(\hat{\boldsymbol{k}}\cdot\Delta\boldsymbol{k})^2}{2k}\right) + \frac{1}{2}\frac{\partial^2\omega}{\partial k^2}(\hat{\boldsymbol{k}}\cdot\Delta\boldsymbol{k})^2 + \ldots \tag{14}$$

or, with $q_\parallel = \hat{\boldsymbol{k}}\cdot\Delta\boldsymbol{k}$ and $\Delta k^2 = q_\parallel^2 + q_\perp^2$, the relation

$$\Delta\omega = \frac{3\omega}{2k}q_\parallel + \frac{3\omega}{4k^2}q_\perp^2 + \frac{3\omega}{8k^2}q_\parallel^2 + \ldots. \tag{15}$$

The resulting equation of motion for a_j is given as (this result has the same form as the expression reported by Ezerskii *et al.* (1986), but we find different values for the coefficients $T_{jk}^{(i)}$ for the case they consider, namely square patterns.):

$$\begin{aligned} 0 = \dot{a}_j + \frac{\mathrm{i}kf}{4\omega}a_{-j}^* + \frac{3\omega}{2k}(\hat{\boldsymbol{k}}_j\cdot\nabla)a_j - \frac{3\mathrm{i}\omega}{4k^2}\nabla^2 a_j + \frac{3\mathrm{i}\omega}{8k^2}(\hat{\boldsymbol{k}}_j\cdot\nabla)^2 a_j \\ - \mathrm{i}T_{jk}^{(1)}|a_k|^2 a_j - \mathrm{i}T_{jk}^{(2)} a_k a_{-k} a_{-j}^* \end{aligned} \tag{16}$$

with the expressions for $T_{jk}^{(i)}$ relegated to Appendix A. The behaviour of these nonlinear coefficients as a function of the angle between the jth and kth waves is displayed in figure 1.

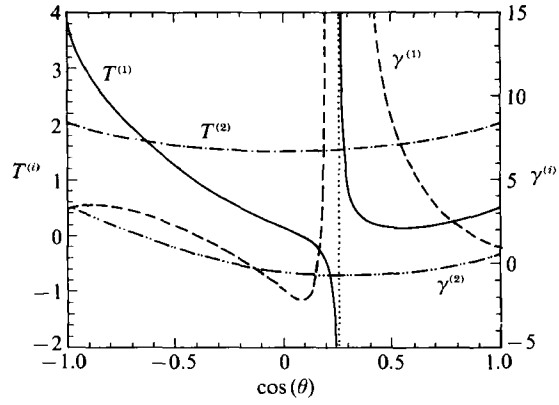

FIGURE 1. The nonlinear frequency-shift coefficients $T^{(i)}_{jk}$ and damping coefficients $\gamma^{(i)}_{jk}$ of the travelling-wave amplitude equations (22) are displayed as a function of $\hat{\boldsymbol{k}}_j \cdot \hat{\boldsymbol{k}}_k$, the cosine of the angle between the jth and kth travelling waves. Solid curve, $T^{(1)}$; dashed curve, $\gamma^{(1)}$; dot-dashed curve, $T^{(2)}$; dot-dot-dashed curve, $\gamma^{(2)}$.

3. Damping

The previous section considered parametrically driven capillary waves in the absence of viscous dissipation. The resulting amplitude equations are Hamiltonian, and in fact are equivalent to an expansion of the total mechanical energy of the system (kinetic plus surface tension) in powers of $\{a_j\}$.

We may add damping in the following way. First note that in the experiments of Tufillaro *et al.* (1989) the viscous penetration or skin depth is much smaller than the wavelength of the capillary waves; hence the flow in the fluid is ideal over almost all of the volume. An argument due to Landau (Landau & Lifshitz 1959) concludes that the contribution to viscous dissipation from within the skin depth is small compared to that in the bulk. So, to compute dissipation in the bulk, we must substitute the computed expansion for the flow, $\phi = \phi_0 + \phi_1 + \phi_2$, into the expression for the viscous dissipation in an incompressible fluid, which is

$$\dot{E} = -2\eta \int \mathrm{d}V \left(\frac{\partial^2 \phi}{\partial x_i \, \partial x_j} \right)^2. \tag{17}$$

The resulting expansion for $\dot{E}$ takes the form

$$\dot{E} = -D^{(0)} |a_j|^2 - D^{(1)}_{jk} |a_j|^2 |a_k|^2 - D^{(2)}_{jk} a_j a_{-j} a^*_k a^*_{-k}, \tag{18}$$

with $D^{(0)} = 8\eta \Sigma k^4$, and explicit expressions for $D^{(i)}_{jk}$, $i = 1, 2$ are relegated to Appendix B.

One may then assume a form for the damping terms in the amplitude equation,

$$\dot{a}_j = -(\gamma^{(0)} + \gamma^{(1)}_{jk} |a_k|^2) a_j - \gamma^{(2)}_{jk} a_k a_{-k} a^*_{-j} + \ldots. \tag{19}$$

Now we take the explicit derivative of the Hamiltonian implied by the amplitude equation, the relevant terms of which are

$$H = h^{(0)} |a_j|^2 + h^{(1)}_{jk} |a_j|^2 |a_k|^2 + h^{(h)}_{jk} a_j a_{-j} a^*_k a^*_{-k} \tag{20}$$

with $h^{(0)} = 2\Sigma k^2$, $h^{(i)}_{jk} = -\Sigma k^4 T^{(i)}_{jk}$ for $i = 1, 2$. (The quadratic part of the Hamiltonian H gives the trivial part of the equation of motion for a_j, namely $\dot{a}_j = -\mathrm{i}\omega a_j$, which has been absorbed into the time-dependent of a_j.)

Equating the two expressions for the dissipation results in $\gamma \equiv \gamma^{(0)} = 2\nu k^2$, and the following results for the $\gamma_{jk}^{(i)}$:

$$\gamma_{jk}^{(i)} = D_{jk}^{(i)}/(2h^{(0)}) - D^{(0)}h_{jk}^{(i)}/(h^{(0)})^2. \tag{21}$$

The behaviour of this nonlinear coefficient as a function of the angle between the jth and kth waves is shown in figure 1. Some comments about these functions are in order. First, though individual coefficients $\gamma^{(i)}$ take on negative values for some angles, this does not lead to negative values for the nonlinear contribution to the energy dissipation. Second, the divergence of $T^{(1)}$ and $\gamma^{(1)}$ at $\cos\theta \sim \frac{1}{4}$ results from a shortcoming of the computational method. For an angle such that $\boldsymbol{k}_1 + \boldsymbol{k}_2$ has length twice $\boldsymbol{k}_0$, a quadratic nonlinearity produces waves at the drive frequency which are resonant, i.e. satisfy the dispersion relation. Because equations of motion for these waves were not retained in the calculation, spurious divergences appear in the coefficients. This leads to divergent damping of pairs of waves separated by an angle of $\theta = \cos^{-1}(2^{\frac{1}{3}} - 1) \approx 74.9°$.

The complete equation of motion for the travelling wave amplitudes then takes the form

$$0 = \dot{a}_j + \gamma^{(0)}a_j + \frac{\mathrm{i}kf}{4\omega}a_{-j}^* + \frac{3\omega}{2k}(\hat{\boldsymbol{k}}_j\cdot\boldsymbol{\nabla})a_j - \frac{3\mathrm{i}\omega}{4k^2}\nabla^2 a_j + \frac{3\mathrm{i}\omega}{8k^2}(\hat{\boldsymbol{k}}_j\cdot\boldsymbol{\nabla})^2 a_j$$
$$+ (\gamma_{jk}^{(1)} - \mathrm{i}T_{jk}^{(1)})|a_k|^2 a_j + (\gamma_{jk}^{(2)} - \mathrm{i}T_{jk}^{(2)})a_k a_{-k} a_{-j}^*. \tag{22}$$

(We have neglected for simplicity the wavenumber dependence of the damping coefficients, which by an extension of the above method would lead to an expansion in gradients of the linear damping term as $\gamma^{(0)}(1 + 3(\hat{\boldsymbol{k}}\cdot\boldsymbol{\nabla})^2/k_0^2)a_j$ at this order. These corrections are small because the relative wavenumber shift is small in the region of interest.)

To summarize: we have explicitly computed the coefficients of this amplitude equation, including both nonlinear frequency shifts ($T_{jk}^{(i)}$) and nonlinear damping ($\gamma_{jk}^{(i)}$), by the systematic expansion of Newell & Whitehead (1969), for an *arbitrary* set of pattern wavevectors $\{\boldsymbol{k}_i\}$. The expressions for the nonlinear coefficients may be found in Appendices A and B. The dependence on $\hat{\boldsymbol{k}}_j\cdot\hat{\boldsymbol{k}}_k$ of these coefficients is shown in figure 1. In the next sections, we shall make use of these general results to examine the local and global stability of regular patterns of capillary waves.

4. Standing waves

The amplitude equations with damping terms are not Hamiltonian; rather, they are derivable from a Hamiltonian plus the dissipation functional (18). Most important, they are not of 'relaxational' form; thus in general we cannot make simple arguments about the most stable state of the driven system as the extremum of some functional.

The presence of damping splits the degeneracy at threshold between the growth rates of the two neutral eigenmodes at each k_j (two degenerate standing waves); for $f = \gamma$, the growth rate of the favourable standing wave just becomes positive, while the other is -2γ.

Thus sufficiently close to threshold (now at $f = \gamma$), the number of relevant neutral modes is half the number of travelling waves. This suggests deriving equations for the amplitudes of standing waves, i.e. applying the Newell–Whitehead formalism anew to the PDEs for the $\{a_j\}$. In particular, we may write new neutral modes as

proportional to the neutral eigenstates of the linearized a_j equations (as in Riecke 1990).

In this way we are led to examine the neutral stability curve of the a_j equations with damping. The linearized equations coupling a_j and a_{-j}^*, which we assume to vary in space as $\exp(\mathrm{i}\boldsymbol{q}\cdot\boldsymbol{x})$ (i.e. we examine the growth of modes slightly different in wavenumber from k), are

$$0 = \begin{bmatrix} -\mathrm{i}\omega+\gamma-\mathrm{i}\sigma & -\mathrm{i}f \\ \mathrm{i}f & -\mathrm{i}\omega+\gamma+\mathrm{i}\sigma \end{bmatrix} \begin{bmatrix} a_j \\ a_{-j}^* \end{bmatrix}. \tag{23}$$

Here the 'detuning' σ is given by $\sigma = -\Delta\omega(q) \approx -(\partial\omega/\partial q)\,\Delta k$. That is, the detuning is the difference in frequency between the subharmonic of the drive, and the natural frequency of a wave with wavevector $\boldsymbol{k}_j+\boldsymbol{q}$.

With the drive strength f at the threshold value $f^* = (\gamma^2+\sigma^2)^{\frac{1}{2}}$, which defines the neutral stability curve in the (f,σ)-plane, the linearized equations have eigenvalues $\mathrm{i}\omega = 0$ and $\mathrm{i}\omega = 2\gamma$. The corresponding eigenvectors are $(1, \mathrm{i}Q)$ and $(\mathrm{i}, -\mathrm{i}Q^*)$ respectively. Here the phase Q is given by

$$Q \equiv \left(\frac{\gamma-\mathrm{i}\sigma}{\gamma+\mathrm{i}\sigma}\right)^{\frac{1}{2}}. \tag{24}$$

Hence the distinction between the two standing waves is their temporal phase with respect to the drive, since

$$\zeta = (a_j \exp(\mathrm{i}\boldsymbol{k}_j\cdot\boldsymbol{x}) + a_{-j}\exp(-\mathrm{i}\boldsymbol{k}_j\cdot\boldsymbol{x}))\exp(-\mathrm{i}\omega t), \quad \text{or} \quad \zeta \propto \cos(\boldsymbol{k}_j\cdot\boldsymbol{x})\exp(-\mathrm{i}\omega t+\mathrm{i}\theta_t),$$

where $\exp(2\mathrm{i}\theta_t) = \mathrm{i}Q$ for the neutral mode and $\exp(2\mathrm{i}\theta_t) = -\mathrm{i}Q^*$ for the decaying mode.

The neutral modes may thus be written

$$(a_j, a_{-j}^*) = (1, \mathrm{i}Q)\,A_j(X,T)\exp(\mathrm{i}\boldsymbol{q}\cdot\boldsymbol{x}). \tag{25}$$

The derivation of the standing-wave amplitude equations is straightforward to third order, as there is no second-harmonic generation, no complications due to a free boundary, and no subsidiary equations to solve. It will turn out that we are interested in σ of $O(\gamma^2)$. For $\sigma \ll \gamma$ we obtain to third order

$$0 = \dot{A}_j - \frac{\sigma}{\gamma}\left(-\frac{3\mathrm{i}\omega}{2k}(\hat{\boldsymbol{k}}_j\cdot\boldsymbol{\nabla}) + \frac{3\omega}{8k^2}(\hat{\boldsymbol{k}}_j\cdot\boldsymbol{\nabla})^2 - \frac{3\omega}{4k^2}\nabla^2\right)A_j - \frac{1}{2\gamma}\left(\frac{3\omega}{2k}(\hat{\boldsymbol{k}}_j\cdot\boldsymbol{\nabla})\right)^2 A_j$$
$$-\left(-\gamma\epsilon+\frac{\sigma^2}{2\gamma}\right)A_j + \left(\Gamma_{jk}+\frac{\sigma}{\gamma}T_{jk}\right)|A_k|^2 A_j, \tag{26}$$

where $T_{jk} \equiv T_{jk}^{(1)} + T_{j-k}^{(1)} + T_{jk}^{(2)} + T_{j-k}^{(2)}$, and Γ similarly in terms of the $\gamma^{(i)}$, and the dimensionless drive strength $\epsilon \equiv (f-\gamma)/\gamma$. (This ϵ is unrelated to the bookkeeping parameter of §2, which will not appear further in this paper.)

Here, as throughout the discussion of the A_j equation, indices in implied sums run only over 'positive' values of the index k; i.e. each wavevector appears only once.

Again we may make a few comments about the structure of the A_j equations.

(i) The linear terms are of the form

$$\left[-\gamma\epsilon+\frac{1}{2\gamma}(\Delta\omega(\boldsymbol{\nabla})-\sigma)^2\right]A_j; \tag{27}$$

systematic expansion to higher order reproduces successive terms in the expansion of $\Delta\omega$ in gradients.

(ii) The cubic term above can *change sign* for sufficiently negative σ, suggesting the need for a fifth-order term. By carrying the expansion to higher order, the fifth-order term can be obtained (for $\sigma \ll \gamma$) as

$$\frac{1}{4\gamma}[(T^{(1)}_{jk}+T^{(1)}_{-jk})\,T_{jl}+(T^{(2)}_{jk}+T^{(2)}_{-jk})\,(2T_{kl}-T_{jl})]\,|A_k|^2\,|A_l|^2\,A_j. \tag{28}$$

The amplitude equation at cubic order is derivable from a Lyapunov functional; the $O(A^5)$ term is not in general derivable from a functional. Sufficiently near to threshold, where the $O(A^5)$ term may be neglected, we may determine the most stable state. To $O(A^4)$, the functional is (omitting gradient terms)

$$F=\left(-\gamma\epsilon+\frac{\sigma^2}{2\gamma}\right)|A_j|^2+\frac{1}{2}\left(\Gamma_{jk}+\frac{\sigma}{\gamma}T_{jk}\right)|A_j|^2\,|A_k|^2. \tag{29}$$

We now suppose a regular pattern (all $|A_j|$ equal). Under the assumption that a mechanism exists for the system to adjust wavelength (hence detuning) continuously, we may minimize F with respect to σ to find the best detuning for a given amplitude, as $\sigma^* = -\frac{1}{2}T|A|^2$ with $T \equiv \Sigma_k T_{jk}$. (For square patterns, we have from Appendix A that $T = 11.79\omega k^2$.)

Of course, it is possible that the system arrives at a pattern in which different standing waves have different amplitudes, or even different detunings; these possibilities may be investigated on the basis of the standing-wave amplitude equations (26), (28) (generalized to the case of different detunings σ_j for the different waves), even in the case when no functional exists. This possibility will not be pursued here.

Proceedings under the assumption of a regular pattern, and disregarding for the moment the small negative term of $O(A^6)$ which is generated, the optimized functional is

$$F(A,\sigma^*(A)) = -\gamma\epsilon nA^2+\tfrac{1}{2}n\Gamma A^4, \tag{30}$$

where $\Gamma \equiv \Sigma_j \Gamma_{jk}$, and h is the number of modes in the pattern. As the summands Γ_{jk} depend on the angle between rolls, Γ takes different values for each regular pattern. The functional (30) has the deepest minimum for a square pattern, among the choices of single waves (rolls), square patterns, or hexagonal patterns. For rolls ($n = 1$), $\Gamma = 6\nu k^4$; for squares ($n = 2$), $\Gamma = 1.93\nu k^4$; and for hexagons ($n = 3$), $\Gamma = 32.29\nu k^4$. (Here ν is the kinematic viscosity.)

The optimum amplitude A for a given drive is then (neglecting $O(A^6)$ terms)

$$A^2=\frac{\gamma\epsilon}{\Gamma},\quad \sigma^*=-\frac{1}{2}\frac{T\gamma\epsilon}{\Gamma}. \tag{31}$$

Nonlinear damping, neglected by Ezerskii *et al.* (1986), thus enters in an essential way to determine the stable amplitude. With the detuning parameter σ to be determined not by the experimenter but by the system through its choice of wavenumber, we require $\Gamma > 0$ to have a finite response to drive strength just above threshold.

Farther from threshold, where the $O(A^6)$ term in F matters, we may still have a functional in a limited sense, under the assumption that the pattern is regular and of a known number of modes. With this strong restriction we may determine the optimal state, i.e. the angle between standing waves, the best value of σ, and the optimum amplitude. This is useful for analysing the stability of a square pattern with respect to a shearing distortion, as well as the behaviour of $\sigma^*(\gamma\epsilon)$ for larger drive amplitudes.

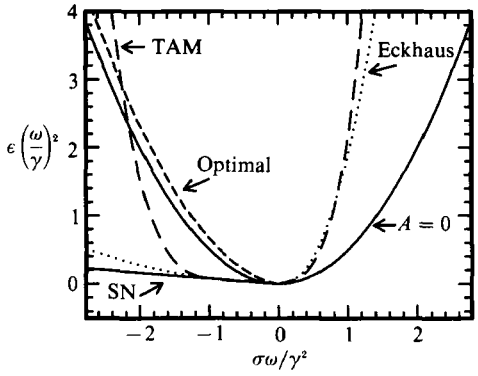

FIGURE 2. Shown are the various stability boundaries in the (ϵ, σ)-plane together with the path of the most stable uniform square pattern. Solid parabola, neutral stability boundary ($A = 0$); solid line, locus of saddle node bifurcations (SN); long dashes, transverse-amplitude instability boundary (TAM); dotted line, Eckhaus instability boundary (Eckhaus); short dashes, the most stable uniform state, $\sigma^*(\epsilon)$ (optimal). The most stable uniform state collides with the TAM boundary.

Under these assumptions, the functional becomes

$$F(A,\sigma) = -\gamma\epsilon n A^2 + \frac{1}{2\gamma}(\sigma + \tfrac{1}{2}TA^2)^2 nA^2 + \tfrac{1}{2}n\Gamma A^4 + \frac{1}{24\gamma} nT^2 A^6. \tag{32}$$

The optimum detuning is $\sigma^* = -\frac{1}{2}TA^2$ as before; the optimum A is the solution of $\partial F/\partial A^2 = 0$, or

$$A^{*2} = \frac{-\Gamma + (\Gamma^2 + \frac{1}{2}\epsilon T^2)^{\frac{1}{2}}}{T^2/4\gamma}. \tag{33}$$

We may then compute the depth of the minimum in F as a function of angle between standing waves in a canted square pattern, using the results of Appendices A and B for T and Γ as functions of the angle between the waves. We find that the square pattern is indeed stable to changes in the angle away from $\frac{1}{2}\pi$. The trajectory of the optimal detuning σ^* as a function of drive strength is displayed in figure 2.

The functional of (32), valid for regular patterns, has a saddle-node bifurcation when the fourth-order term has a negative coefficient, or $\sigma T/\gamma + \Gamma < 0$. (See figure 2.) The saddle node occurs when the drive decreases to the point at which F loses the pair of extrema which are associated with the metastable state at finite amplitude A. This occurs when

$$\gamma\epsilon = -\frac{\Gamma^2\gamma}{2T^2} - \frac{\sigma\Gamma}{T}. \tag{34}$$

The finite-amplitude uniform solution becomes metastable on a transition line at a slightly higher value of drive. Between the neutral stability boundary and the transition line, the $A = 0$ uniform solution is metastable.

Perhaps unfortunately, it is not evident that the physical system may be constrained to respond to the drive with patterns of a given wavelength, corresponding to some desired detuning σ. Left to its own devices, the system is free to choose $\sigma = \sigma^*(\gamma\epsilon)$, which avoids the region of metastability. (The detuning parameter σ, which was undetermined and phenomenological in the work of Ezerskii *et al.* (1986), is in fact given by minimizing the functional of (32).)

5. Secondary instabilities

Following standard methods, we may find the boundaries of stability of the uniform pattern of the standing-wave amplitude equations by searching for transverse (zigzag) and longitudinal (Eckhaus) instabilities (Eckhaus 1965). We know the relation between detuning and amplitude, from the functional valid for square patterns; and, from the equation for stationarity of the pattern, we have the expression for drive in terms of detuning and amplitude. Thus we know the path of the most stable square uniform state in the (ϵ, σ)-plane. One can then check to see whether the path collides with a stability boundary.

It turns out that the path collides not with an Eckhaus boundary, but rather with a boundary for a transverse amplitude modulation (TAM) instability, described by Ezerskii *et al.* (1986). The TAM instability is *not* found in the standing-wave equations but rather in the full travelling-wave amplitude equations, for the following reason. The standing-wave equations were derived essentially by assuming that the decaying, non-neutral combination of travelling waves was a degree of freedom whose amplitude was slaved to the neutral mode, i.e. that its dynamics were adiabatic. The full travelling-wave equations for the a_j are (since a_j and a_{-j}^* are coupled) second order in time, while the standing-wave equations omit half of the modes and are first order in time. The TAM instability explicitly involves the dynamics of the decaying standing wave, and hence the breakdown of the adiabatic approximation which gave rise to the standing-wave equations. This secondary instability thus answers the question of how the system, at some drive f above threshold, reintroduces the degrees of freedom which were irrelevant at smaller f.

We linearize about the stationary solution of the standing-wave equation (with fifth-order terms included), i.e. the minimum of the functional of (32), which satisfies

$$0 = -\gamma\epsilon + \frac{\sigma^2}{2\gamma} + \left(\Gamma + \frac{\sigma T}{\gamma}\right) A_\sigma^2 + \frac{T^2}{2\gamma} A_\sigma^4. \tag{35}$$

We perturb the jth standing wave by writing $A_j = A_\sigma + (B' + iB'')$, where B' and B'' are small space- and time-dependent perturbations on the uniform wave amplitude A_σ, and $A_k = A_\sigma$ for $k \neq j$. With the jth roll taken along $\hat{x}$, this leads to

$$\left.\begin{aligned} 0 &= \dot{B}' + \frac{1}{2\gamma}\left[-\tfrac{9}{4}\partial_x^2 + \tfrac{9}{16}\partial_y^4 + \tfrac{3}{2}\sigma\partial_y^2\right]B' - \frac{3\sigma}{2\gamma}\partial_x B'' + 2\left[\left(\Gamma_{jj} + \frac{\sigma}{\gamma}T_{jj}\right)A_\sigma^2 + \frac{\bar{T}^2}{\gamma}A_\sigma^4\right]B', \\ 0 &= \dot{B}'' + \frac{1}{2\gamma}\left[-\tfrac{9}{4}\partial_x^2 + \tfrac{9}{16}\partial_y^4 + \tfrac{3}{2}\sigma\partial_y^2\right]B'' - \frac{3\sigma}{2\gamma}\partial_x B'', \end{aligned}\right\} \tag{36}$$

with *no* implied sum on j, and where $\bar{T}^2$ is given by

$$\bar{T}^2 \equiv T_{jj}T + \sum_f (T_{jf}^{(2)} + T_{-jf}^{(2)})(T_{jf} - T_{jj}). \tag{37}$$

For square patterns, the values of these coefficients are computed from Appendices A and B to be $\bar{T} = 9.19\omega k^2$, $T_{jj} = 1.33\omega k^2$, and $\Gamma_{jj} = 4.82\nu k^4$.

As usual, the B' and B'' are decoupled in the case of modulations transverse to the wavevector $\boldsymbol{k}_j$ of the roll we are perturbing ($\partial_x \to 0$), and coupled in the longitudinal case. The transverse case gives a phase instability for $\sigma > 0$. The longitudinal case gives an Eckhaus instability when

$$\frac{\sigma^2}{\gamma} > A_\sigma^2\left(\Gamma_{jj} + \frac{\sigma}{\gamma}T_{jj}\right) + \frac{\bar{T}^2}{\gamma}A_\sigma^4. \tag{38}$$

As a matter of numerical convenience, the Eckhaus boundary may be plotted in the (ϵ, σ)-plane parametrically as a function of A, by solving (38) for $\sigma(A)$, and computing $f(A, \sigma(A))$ from the stationarity condition for a finite-amplitude pattern,

$$f^2 = (\gamma + \Gamma A^2)^2 + (\sigma + TA^2)^2. \tag{39}$$

(See figure 2.)

Some comments on the unusual shape of the Eckhaus boundary are in order. Very near threshold, where the last term of (36) may be approximated by $2\Gamma_{jj} A_\sigma^2 B'$ and (35) similarly approximated, the Eckhaus boundary and neutral stability curves are given respectively by

$$\frac{\sigma^2}{2\gamma} \approx \frac{\Gamma_{jj}}{2\Gamma + \Gamma_{jj}} \delta f, \quad \frac{\sigma^2}{2\gamma} \approx \delta f.$$

Thus the usual factor of $\frac{1}{3}$ is replaced in this limit by $\Gamma_{jj}/(2\Gamma + \Gamma_{jj})$ when dealing with patterns with more than one set of waves.

The asymmetry of the Eckhaus boundary occurs in the vicinity of the emergence of the line of saddle nodes (see §4). This occurs at $\sigma/\omega = -(\gamma/\omega)(\Gamma\omega/\gamma T)$ which for square patterns is $-0.16\gamma/\omega$.

Observe finally that the optimal-state trajectory does not cross the Eckhaus boundary; this is intuitive, since the Eckhaus instability is a mechanism for the system to locally adjust the wavenumber when global adjustment is impossible.

The instability analysis of the full a_j equations is much more complicated, because the linearized equations result in a 4×4 system in the general case. However, in the case of disturbances of one standing wave in a pattern transverse to its wavevector $\boldsymbol{k}_j$, the linearized equations decouple into two 2×2 systems. One system describes the coupling of spatial phase and relative amplitude degrees of freedom for left-and right-moving parts of the standing wave, and gives in the long-wavelength limit an 'undulation' or transverse phase modulation mode, already encountered above.

The second 2×2 system describes the dynamical coupling of temporal phase and overall amplitude degrees of freedom of the left- and right-moving waves, and gives rise to the transverse amplitude modulation (TAM) instability, which is not present in the A_j equations. It can be shown explicitly that the series of corrections to the standing-wave neutral mode (equation (25)) generated in the Newell–Whitehead-type derivation of the standing-wave equations is the same as an adiabatic approximation on the dynamics of the temporal phase in the travelling-wave equations (16), (17).

We linearize about the stationary solutions of (22), perturbing the jth travelling wave by writing $a_{\pm j} = \exp(\mathrm{i}\theta_t)(A + b_{\pm j})$, and $a_{\pm j} = \exp(\mathrm{i}\theta_t)A$ for $k \neq j$. The decoupling of the 4×4 equations for the real and imaginary parts of $b_{\pm j}$ is achieved by a simple change of variable. Defining $b \equiv b_j + b_{-j}$, we obtain

$$0 = \dot{b}' + \frac{3\omega}{4k^2} \nabla_\perp^2 b'' + 2(\sigma + T_1 A^2) b'' + 2\Gamma_2 b', \tag{40}$$

$$0 = \dot{b}'' - \frac{3\omega}{4k^2} \nabla_\perp^2 b' + 2(\gamma + \Gamma_1 A^2) b'' - 2T_2 A^2 b', \tag{41}$$

where we have defined

$$T_1 \equiv \sum_k T_{jk}^{(1)} + T_{jj}^{(2)} + T_{-jj}^{(2)}, \quad T_2 \equiv T_{jj}^{(1)} + T_{jj}^{(1)} + T_{jj}^{(2)} + T_{-jj}^{(2)},$$

and similarly for Γ_i in terms of $\gamma^{(l)}$. For square patterns, the values of these coefficients computed from Appendices A and B are $T_1 = 8.79\omega k^2$, $T_2 = 8.5\omega k^2$, $\Gamma_1 = 2.94\nu k^4$, and $\Gamma_2 = 6\nu k^4$.

The condition for (40), (41) to give positive growth rates for disturbances is

$$4\Gamma_2 A^2(\gamma+\Gamma_1 A^2)+\left(\frac{3\omega}{4k^2}q^2-(T_1+T_2)A^2-\sigma\right)^2-(\sigma+(T_1-T_2)A^2)^2<0. \tag{42}$$

If $\sigma+(T_1+T_2)A^2>0$, then the left-hand side of the inequality is smallest for instabilities at wavenumber q given by

$$\frac{3\omega}{4k_2}q^2=(T_1+T_2)A^2+\sigma. \tag{43}$$

Otherwise, the least stable $\boldsymbol{q}$ is $\boldsymbol{q}=0$; this leads to an instability for $\sigma<-(T_1+T_2)A^2$ when $\sigma<-T_1A^2-T_2^{-1}\Gamma_2(\gamma+\Gamma_1)A^2$. This is never satisfied for the optimal state.

Just as for the Eckhaus boundaries, (38), the limits of (42) may be conveniently plotted by solving for σ,

$$\sigma_\pm=-(T_1-T_2)A^2\pm[4\Gamma_2A^2(\gamma+\Gamma_1A^2)]^{\frac{1}{2}}, \tag{44}$$

and plotting $\gamma\epsilon(\sigma)$ parametrically as a function of A. (See figure 2.)

We may find analytically the location of the crossing of the optimal state, (33) with $\sigma^*=-\frac{1}{2}TA^2$, and the left-hand TAM boundary, for $\gamma\ll\omega$; this occurs at

$$\left.\begin{aligned}\sigma&=\frac{-2T\gamma\Gamma_2}{(T_1-T_2-\frac{1}{2}T)^2},\\ f^2&=\gamma^2+\frac{8\gamma^2\Gamma_2\Gamma}{(T_1-T_2-\frac{1}{2}T)^2}+\frac{4T^2\gamma^2\Gamma_2^2}{(T_1-T_2-\frac{1}{2}T)^4},\\ A^2&=\frac{4\gamma\Gamma_2}{(T_1-T_2-\frac{1}{2}T)^2}.\end{aligned}\right\} \tag{45}$$

Note that at this point, all terms in the standing-wave functional F of (32) are of the same order. Terms not calculated in F, of higher order in A/γ, would all be of comparable magnitude. Hence the numerical values of the coefficients of (45) may not be reliable.

Proceeding with the calculated values for the various coefficients, the secondary instability occurs at a drive strength above threshold $(f^2-\gamma^2)/\gamma^2=2\epsilon=5.81(\gamma/\omega)^2$, with a detuning $\sigma/\omega=2.25(\gamma/\omega)^2$, an amplitude $kA=0.618\gamma/\omega$, and a modulational wavenumber $q/k=2.41\gamma/\omega$.

For presenting the locations of the various stability boundaries in the (ϵ,σ)-plane, we note that for $\gamma\ll\omega$, we may scale $kA=A'(\gamma/\omega)$, $\Gamma=\Gamma'\gamma k^2$, $\sigma/\omega=\sigma'(\gamma/\omega)^2$, and $\epsilon=\epsilon'(\gamma/\omega)^2$, and all dependence on γ and ω scales out (with corrections of order $(\gamma/\omega)^2$). The resulting neutral stability, saddle node, Eckhaus, and TAM boundaries are shown together with the optimal state trajectory in figure 2.

6. Conclusion

6.1. *Summary of theory*

We have derived two different amplitude equations to describe the evolution of general patterns in parametrically driven capillary wave systems. The first amplitude equation is for travelling capillary waves, which are the neutral modes in the absence of dissipation, with a vanishing threshold drive strength. These equations are systematically obtained in an expansion in the width of the band of excited modes, following Newell & Whitehead (1969). Ezerskii *et al.* (1986) previously presented

these equations for the particular case of square patterns; we agree as to the form of these amplitude equations but disagree as to the values of the coefficients for square patterns.

To these Hamiltonian equations we add both linear and nonlinear damping terms, which are calculated from the viscous dissipation of energy in the bulk of the fluid, expanded in powers of the travelling wave amplitudes, using the flow field results of the amplitude equation expansion. (Only linear damping terms are present in the work of Ezerskii *et al.* (1986); it turns out that the nonlinear terms play an essential role in selecting the square pattern, see below.) The resulting equations are not derivable from a functional, and thus may have dynamics which is not merely relaxational; one may not infer from these equations in any simple way the most stable uniform pattern.

The effect of viscous damping is to split the degeneracy of the growth rates of the two standing waves (which are both neutral modes as zero drive in the absence of damping), resulting in two standing capillary waves with different growth rates. Riecke (1990) observed in a recent paper that for drive strengths sufficiently near the threshold for the faster-growing mode, the dynamics of the slow-growing mode may be adiabatically eliminated. We employ this idea to obtain a second amplitude equation, for standing waves, with half the number of degrees of freedom of the first amplitude equation. This second equation is derivable from a functional (for drive strength near enough to threshold); thus, the most stable uniform pattern and its wavenumber may be found.

The quartic term in the corresponding functional is a measure of the strength of non-linear damping, which enters is an essential way in determining the most stable pattern. We find that square patterns (which are observed experimentally) are preferred among rolls, squares, and hexagonal patterns. The basic reason for this is that square patterns have the weakest nonlinearity in the damping, which allows the functional to attain the deepest minimum (and the pattern amplitude to grow the largest).

We examine each set of amplitude equations for secondary instabilities; the standing-wave equations have the usual longitudinal Eckhaus and transverse phase instabilities (Eckhaus 1965; Newell & Whitehead 1969). However, patterns of the full travelling-wave equations have a transverse amplitude modulation (TAM) instability, described by Ezerskii *et al.* (1986). We find that the uniform pattern which minimizes the functional from which the standing wave equations are derived collides with the TAM instability boundary, and compute the drive strength $(f-\gamma)/f = \epsilon$, instability wavenumber $\boldsymbol{q}$, and pattern amplitude A for which this occurs. For weak damping ($\gamma/\omega \ll 1$), the quantities $(kA)^2$, $(q/k)^2$, and ϵ all scale as $(\gamma/\omega)^2 \sim \nu^2(\rho/\Sigma)^{\frac{4}{3}}\omega^{\frac{2}{3}}$.

6.2. *Comparison with experiment*

Two recent experiments on parametrically driven capillary waves (Douady & Fauve 1988; Tufillaro *et al.* 1989) are candidates for comparison to the present theory of systems of large aspect ratio, in which viscous damping at the walls and the free surface of the fluid are neglected, as are effects due to a discrete spectrum of excitable modes. We review in Appendix C the various boundary contributions to damping which are neglected in the present calculation, to determine which of the experiments may sensibly be compared with the present theory.

We conclude that the system of Tufillaro *et al.* (1989) is indeed large enough that dissipation at the walls of the container may be neglected. We find that surface contamination could possibly contribute appreciably to the damping, but no history

dependence has been reported (J. P. Gollub 1989, private communication) for measurements on n-butyl alcohol used in these experiments. If nonlinear surfactant damping were important, its dependence on the angle between waves would have to be investigated to preserve the conclusions of §4 as to the global stability of square patterns.

The experiments of Douady & Fauve (1988) may not satisfy the assumptions of the present theory that the damping is confined to the bulk of the fluid. Using the experimental parameters, we find that the ratio of dissipation at the walls of the container to the bulk contribution is about 0.25, which may be neglected; and there is no contribution to dissipation from a moving contact line, since the meniscus is pinned in these experiments. However, the surface of the water used in these experiments is intentionally contaminaed with surface-active molecules to stabilize the surface tension. This may lead to large surface contributions to the damping. As evidence of this, the threshold for the initial instability is reported to be about 200 cm/s^2, while the theoretical prediction assuming only bulk damping is about 60 cm/s^2.

More important may be the effects of a discrete spectrum in the experiments of Douady & Fauve (1988). They observe in systems of smaller aspect ratio ($L \sim 10\lambda$) a great variety of possibly metastable states. First, they observed 'symmetric' superpositions of eigenstates $\sin(n\pi x/L)\sin(m\pi y/L)$ and $\sin(m\pi x/L)\sin(n\pi y/L)$ with n and m ranging from 1 to about 15. These may be regarded as four rolls of equal amplitude with wavevectors $\boldsymbol{k} = n\hat{\boldsymbol{x}} \pm m\hat{\boldsymbol{y}}$ and $m\hat{\boldsymbol{x}} \pm n\hat{\boldsymbol{y}}$. Second, they observed 'dissymmetric' states of a single eigenstate $\sin(n\pi x/L)\sin(m\pi y/L)$, i.e. two rolls of equal amplitude and wavevectors $\boldsymbol{k}_\pm = m\hat{\boldsymbol{x}} \pm n\hat{\boldsymbol{y}}$ for angles between $\boldsymbol{k}_+$ and $\boldsymbol{k}_-$ greater than $\frac{1}{4}\pi$.

Douady & Fauve (1988) report that the modes with the smallest values of m, i.e. those most nearly square (with the least overall modulation), have the largest existence domain in frequency; this may be consistent with the global stability of the square pattern in a large system. They also reports that the threshold drive is lowest for the smallest ratio m/n for m^2+n^2 constant; this is indicative of finite-system effects, since the threshold drive in a large system does not involve nonlinear effects, and depends only on frequency (and not, for example, on pattern symmetry).

The present theory predicts that such finite-m states are not globally stable, in the absence of boundary effects (including discrete spectrum effects). In particular, the 'dissymmetric' states correspond to canted square patterns which the present work shows are not globally stable. The metastability of these states could be investigated by repeating the analysis of §5 for these non-square patterns.

With high-viscosity fluids (e.g. glycerol), Douady & Fauve (1988) observe an essentially hexagonal pattern. For this case, the viscous penetration depth l is such that $kl \gtrsim 1$; most of the viscous damping is within the skin depth, and the present calculation of the frequency shift parameters $T_{jk}^{(i)}$ and nonlinear damping coefficients $\gamma_{jk}^{(i)}$, which assume $kl \ll 1$, are not valid.

Our predictions for the primary and secondary instabilities are in qualitative agreement with the experiments of Tufillaro *et al.* (1989); the quiescent state gives way to a square pattern, which for slightly higher drive becomes unstable to transverse amplitude modulation (TAM) of the standing waves in the pattern. However, there are quantitative discrepancies. With experimental parameters $\omega = 320\pi$, $\nu = 0.03$, $\pi = 0.8$, and $\Sigma = 24$ (c.g.s. units), they measure a threshold acceleration amplitude $f^* = 5.4g$. This is *lower* than the theoretical value of $f^* = 4\omega\gamma/k = 8g$.

This discrepancy cannot be due to damping processes not included in the theory, which would lead to an experimental threshold higher than the predicted one. The discrepancy may be due to non-uniform acceleration of the container; the displacement at threshold is only 9 μm. A direct measurement of γ from the decay time of free oscillations is difficult because of the finite response time of the electromagnetic shaker used to produce the waves (J. P. Gollub 1989, private communication). (In the experiments of Ezerskii *et al.* (1986), the observed threshold is reported as $f^* = 4.2\,g$, *higher* than the appropriate theoretical value of $2.8\,g$. Ezerskii *et al.* (1986) claim good agreement without explicitly making the comparison.)

The transverse amplitude modulation (TAM) instability, first observed by Ezerskii *et al.* (1985, 1986), is indeed exhibited in the experiments of Tufillaro *et al.* (1989). In their experiments, the TAM instability occurs experimentally at $\epsilon = 0.10$, compared to the theoretical prediction of $\epsilon = 0.01$. This could be explained by nonlinear damping coefficients which were a factor of three higher than the values predicted from bulk damping only. The corresponding values of pattern amplitude $\zeta_{\max} = 8A$, instability wavenumber q, and frequency detuning σ (a measure of the wavenumber shift of the pattern from its threshold value) are in better agreement with experiment. The theoretical values for the parameters of Tufillaro *et al.* are: $\zeta_{\max} = 95\mu$, $k/g = 6.6$, and $\sigma/\omega = 9 \times 10^{-3}$. Experimentally (J. P. Gollub, private communication), $k/q \sim 8$, σ/ω is unmeasurably small, and $\zeta_{\max}$ is consistent with $\sim 100\mu$.

The mechanism for the determination of the globally optimal wavenumber of the square pattern and the eventual TAM instability are robust to changes in the values of the nonlinear coefficients which may result from the importance of higher-order terms in the standing-wave amplitude equation or new damping processes. The scaling of the secondary instability with γ/ω for $\gamma/\omega \ll 1$ is also robust and may be tested by measuring the secondary threshold as a function of frequency (or viscosity, or surface tension).

I am indebted to Boris Shraiman and Pierre Hohenberg for a patient introduction to the subject of nonlinear dynamics, and the suggestion of this problem. I thank Jerry Gollub and R. Ramshankar for many useful discussions of their experiments, and acknowledge helpful conversations with Paul Kolodner, Jim Stokes, and Eric Herbolzheimer. This research was supported in part by the National Science Foundation under Grant No. PHY82-17853, supplemented by funds from the National Aeronautics and Space Administration.

Appendix A. Expansion of $\dot{a}_j$

Here we present some intermediate results of the amplitude equation expansion, including the expressions for $T^{(i)}_{jk}$; the terms in the equation of motion for a_j generated at each order; the non-resonant corrections Ψ_i to the sum of resonant modes Ψ_0; and the particular solutions $\phi^{(p)}_i$.

The expressions for the $T^{(i)}$ are

$$T^{(1)} = \omega k^2 \left[c^2 - 3c - \frac{1}{2} + \frac{(5 - 9c - 16c^2 - 4c^3) - (\frac{1}{2}(1+c))^{\frac{1}{2}}(6 - 14c - 4c^2)}{4 - (2(1+c))^{\frac{3}{2}}} \right], \tag{A 1}$$

$$T^{(2)} = \omega k^2 [\tfrac{3}{2} + \tfrac{1}{2}c^2], \tag{A 2}$$

where $c = \hat{\boldsymbol{k}}_j \cdot \hat{\boldsymbol{k}}_k$ in the above.

The particular solutions $\phi^{(p)}$ used in enforcing incompressibility for spatially varying patterns (when the z-dependence $\exp(kz)$ does not satisfy $\nabla^2\phi = 0$), are:

$$\phi_1^{(p)} = -\frac{\omega z}{k}\exp(kz)\sum_j (\hat{\boldsymbol{k}}\cdot\boldsymbol{\nabla})\,a_j \exp[\mathrm{i}(\boldsymbol{k}_j\cdot\boldsymbol{x}-\omega t)] + \text{c.c.}, \tag{A 3}$$

$$\begin{aligned}\phi_2^{(p)} = {} & \left\{\frac{\mathrm{i}\omega z^2}{2k}(\hat{\boldsymbol{k}}_j\cdot\boldsymbol{\nabla})^2 a_j + \frac{\mathrm{i}\omega z}{2k^2}\left[\nabla^2 a_j - \tfrac{1}{2}(\hat{\boldsymbol{k}}_j\cdot\boldsymbol{\nabla})^2 a_j + \frac{\mathrm{i}fk^2}{4\omega^2}(\hat{\boldsymbol{k}}_j\cdot\boldsymbol{\nabla})\,a_j^*\right]\right\} \\ & \times \exp[\mathrm{i}(\boldsymbol{k}_j\cdot\boldsymbol{x}-\omega t)]\exp kz \\ & + \tfrac{1}{4}\omega z\frac{(1-5c-2c^2)}{(\frac{1}{2}(1+c))^{\frac{1}{2}}[(\frac{1}{2}(1+c))^{\frac{3}{2}}-2)]}[(\hat{\boldsymbol{k}}_j+\hat{\boldsymbol{k}}_l)\cdot\boldsymbol{\nabla}](a_j a_l) \\ & \times \exp[\mathrm{i}((\boldsymbol{k}_j+\boldsymbol{k}_l)\cdot\boldsymbol{x}-2\omega t)]\exp|\boldsymbol{k}_j+\boldsymbol{k}_l|z + \text{c.c.},\end{aligned} \tag{A 4}$$

where in the above $c = \hat{\boldsymbol{k}}_j\cdot\hat{\boldsymbol{k}}_l$.

The non-resonant corrections to $\Psi_0 = (\zeta_0, \phi_0)$ are

$$\begin{aligned}\Psi_1 = {} & -\sum_j \begin{pmatrix} 1 \\ \mathrm{i}\omega/k \end{pmatrix}\left[\frac{-\mathrm{i}}{4k}(\hat{\boldsymbol{k}}_j\cdot\boldsymbol{\nabla})\,a_j + \frac{fk}{8\omega^2}a_j^*\right]\exp[\mathrm{i}(\boldsymbol{k}_j\cdot\boldsymbol{x}-\omega t)] + \text{c.c.} \\ & + \tfrac{1}{2}k\sum_{j\neq l}\begin{pmatrix} 1 \\ 0 \end{pmatrix} a_j^* a_l \exp[\mathrm{i}(\boldsymbol{k}_j-\boldsymbol{k}_l)\cdot\boldsymbol{x}] \\ & + \tfrac{1}{4}k\sum_{jl}\begin{pmatrix} d \\ -\mathrm{i}\omega b/k \end{pmatrix} a_j a_l \exp[\mathrm{i}((\boldsymbol{k}_j+\boldsymbol{k}_l)\cdot\boldsymbol{x}-2\omega t)] + \text{c.c.},\end{aligned} \tag{A 5}$$

where

$$\left.\begin{aligned} d &= d_{jl} \equiv [(\tfrac{1}{2}(1+c))^{\frac{1}{2}}(3-c)-2(1+c)]\,[2(\tfrac{1}{2}(1+c))^{\frac{3}{2}}-1]^{-1}, \\ b &= b_{jl} \equiv [1-5c-2c^2]\,[2(\tfrac{1}{2}(1+c))^{\frac{3}{2}}-1]^{-1}, \\ c &= c_{jl} \equiv \hat{\boldsymbol{k}}_j\cdot\hat{\boldsymbol{k}}_l. \end{aligned}\right\} \tag{A 6}$$

Two terms generated to second order in the expansion of $\dot{a}_j$ not shown in (16) are

$$0 = \dot{a}_j \ldots - \frac{f}{8\omega}(\hat{\boldsymbol{k}}_j\cdot\boldsymbol{\nabla})\,a_{-j}^* - \frac{\mathrm{i}f^2k^2}{32\omega^3}a_j, \tag{A 7}$$

which represent detuning of the driving term and second-order response to the drive, respectively. These terms are both small in the experimental cases of interest, because the drive strength at threshold is $O(\gamma/\omega)$, which is small.

Appendix B. Damping expansion

Equation (16) for the dissipation of energy due to viscous damping in the bulk may be written using incompressibility as

$$-\eta\int \mathrm{d}V\,\nabla^2\left(\frac{\partial\phi}{\partial x_i}\right)^2; \tag{B 1}$$

the limits of integration depend on the wavy free surface of the liquid, and so may be expanded

$$\dot{E} = -\eta\int \mathrm{d}^2x\left[\int_{-\infty}^{0}\mathrm{d}z + \zeta + \tfrac{1}{2}\zeta^2\partial_z + \ldots\right]\nabla^2(\partial_i\phi)^2. \tag{B 2}$$

Integrations by parts leads to

$$\dot{E} = -\tfrac{1}{2}\eta\int \mathrm{d}^2x[\partial_z^3\phi^2 + (\nabla^2+\partial_z^2)^2(\zeta+\tfrac{1}{2}\zeta^2)\phi^2], \tag{B 3}$$

where in the above, ∇^2 acts only on ζ and ∂_z acts only on ϕ, which is evaluated at $z = 0$.

To expand (B 3) to the order required in (18), we must also have the non-resonant cubic correction Ψ_2, which turns out to be

$$\Psi_2 = \sum_{jf} 4\omega k^2 \begin{pmatrix} 1 \\ \mathrm{i}\omega/k \end{pmatrix} \{B_1 a_j |a_f|^2 + B_2 a_f a_{-f} a^*_{-j}\} \exp[\mathrm{i}(\boldsymbol{k}_j \cdot \boldsymbol{x} - \omega t)] + \text{c.c.}, \tag{B 4}$$

where
$$\left.\begin{aligned} B_1 &= 1 - 2c + 2c^2 + (\tfrac{1}{2}(\tfrac{1}{2}(1+c))^{\frac{1}{2}}[5 - 8c - 5c^2 + (1+c)^2(1-\delta)] \\ &\quad - \tfrac{1}{2}(1+c)(1-\delta) - (1+c)^2)(2(\tfrac{1}{2}(1+c))^{\frac{3}{2}} - 1)^{-1}, \\ B_2 &= \tfrac{3}{2} + c^2 + \tfrac{1}{2}(1 - \delta_{-jf}). \end{aligned}\right\} \tag{B 5}$$

In the above, $c \equiv \hat{\boldsymbol{k}}_j \cdot \hat{\boldsymbol{k}}_f$ as before, and $\delta = \delta_{jf}$, the Kronecker delta.

A tedious and straightforward expansion of (B 2) then yields

$$\left.\begin{aligned} D^{(1)} &= -4\nu\omega^2 k^3 [-B_1 + 2b^2(\tfrac{1}{2}(1+c))^{\frac{3}{2}} + 2b(1+c)(1 + (\tfrac{1}{2}(1+c))^{\frac{1}{2}})^2 \\ &\quad - \tfrac{1}{2}d(1-c)^2 + \tfrac{1}{2}(1+c)^2(1-\delta) + 8(1+c)], \\ D^{(2)} &= [-B_2 + \tfrac{1}{2}(1-c)^2(1-\delta_{-jk}) - 2(1-c^2)], \end{aligned}\right\} \tag{B 6}$$

with B_1, B_2, b, d, c, and δ as in (B 5) and (A 6) respectively.

Equation (21) may then be evaluated numerically for any cases of interest. Relevant numerical results for the various damping parameters are given in the main text.

The above procedure may be extended to give damping coefficients which depend on the spatial derivatives of the a_j, terms neglected in the expansion (18) of the energy dissipation. At linear order we obtain finally

$$\dot{a}_j = -2\nu k^2 \left(1 + \frac{3}{16k^2}(\hat{\boldsymbol{k}}_j \cdot \boldsymbol{\nabla})_2\right) a_j + \ldots. \tag{B 7}$$

Rotational invariance arguments require the linear damping of a mode to depend only on its wavenumber, and not on the direction of its wavevector. Hence $(\hat{\boldsymbol{k}}_j \cdot \boldsymbol{\nabla})$ in the above must be replaced in general by $\mathrm{i}\Delta k_j(\boldsymbol{\nabla})$, the expansion of which is

$$\mathrm{i}\Delta k_j(\boldsymbol{\nabla}) = (\hat{\boldsymbol{k}}_j \cdot \boldsymbol{\nabla}) - \mathrm{i}(\nabla^2/(2k) - (\hat{\boldsymbol{k}}_j \cdot \boldsymbol{\nabla})^2/(2k)) + \ldots. \tag{B 8}$$

Thus we have an expansion for $\gamma(\boldsymbol{\nabla})$ which begins

$$\gamma(\boldsymbol{\nabla}) = 2\nu k^2 \left(1 + \frac{3}{16k^2}((\hat{\boldsymbol{k}}_j \cdot \boldsymbol{\nabla}) - \mathrm{i}\nabla_\perp^2/2k)^2\right) + \ldots. \tag{B 9}$$

Appendix C. Damping at boundaries

In addition to the bulk contribution to energy dissipation computed in Appendix B, there are three additional sources of dissipation in a deep cell of finite size L, with some amount of adsorbed surface contaminants present on the free surface. These are (i) damping γ_w at the walls of the container; (ii) damping γ_1 at a moving contact line (meniscus) along the wall of the container; and (iii) damping γ_s due to a surface layer of finite compressibility. We consider each of these in turn, following Miles (1967) and Cox (1986).

At the sidewalls of the container, the fluid velocity changes over a viscous penetration depth $l = (2\nu/\omega)^{\frac{1}{2}}$ from the ideal-fluid bulk value $\boldsymbol{v} = \boldsymbol{\nabla}\phi$ to $\boldsymbol{v} = 0$. Thus velocity gradients are of order l^{-1}; then (17) leads to

$$\dot{E} = (\tfrac{1}{2}\nu\omega)^{\frac{1}{2}} \int \mathrm{d}S' \, v^2, \tag{C 1}$$

where the integral $\int \mathrm{d}S'$ is over the wall surfaces. The integral over depth $\int \mathrm{d}z$ leads to a factor $(2k)^{-1}$, and we may replace v along the wall at $z = 0$ by $k\phi$; this leads to

$$\dot{E}_w = (\tfrac{1}{2}\nu\omega)^{\frac{1}{2}} k^2 \int \mathrm{d}L' \, \phi^2. \tag{C 2}$$

The total energy of small oscillations is twice the kinetic energy, which leads to

$$E = \tfrac{1}{2}\rho k \int \mathrm{d}S \, \phi^2. \tag{C 3}$$

Then the damping coefficient $\gamma_w \equiv \dot{E}/(2E)$ is given by

$$\gamma_w = \omega l / L. \tag{C 4}$$

The ratio of γ_w to the bulk contribution γ to the linear damping coefficient is then $\gamma_w/\gamma = (Llk^2)^{-1}$. For the experiments of Tufillaro *et al.* (1989), where $L = 8$ cm, $\omega/2\pi = 160\ \mathrm{s}^{-1}$, $\nu = 0.03\ \mathrm{cm}^2\ \mathrm{s}^{-1}$, and $\sigma \sim 24\ \mathrm{erg\ cm}^{-2}$, we have $l \sim 8 \times 10^{-3}$ cm, $k = 32\ \mathrm{cm}^{-1}$, and $\gamma_w/\gamma \sim 10^{-2}$.

Dissipation at a moving contact line is a more subtle quantity, as it depends on the microscale at which the no-slip boundary condition is violated; a hydrodynamic description of a moving contact line without slip has a infinite dissipation rate (Bretherton 1961). The slip scale may be set by some combination of molecular lengths and surface roughness, and may vary from material to material. Cox (1986) has analysed the velocity dependence of the contact angle to first order in capillary number Ca. For the case of a viscous fluid displacing air he obtains

$$\Delta\theta = f(\theta)\, \mathrm{Ca} \ln \epsilon^{-1}, \tag{C 5}$$

where $\Delta\theta$ is the velocity-dependent change in the macroscopic contact angle, $f(\theta) = 2\sin(\theta)[\theta - \sin(\theta)\cos(\theta)]^{-1}$, and the capillary number is $Ca = \eta v/\sigma$. The cutoff parameter ϵ is $\epsilon = s/R$, where s is the slip length and R is a macroscopic length at which the surface is no longer flat. For the present case we make a conservative estimate $s = 10$ Å, and $R = l$.

To determine the dissipation at the moving contact line, we may compute the work done by surface tension as the contact angle changes and the contact line moves. This gives a dissipation per unit length of order

$$\dot{E}/L \sim v\sigma[\cos(\theta_0 + \Delta\theta) - \cos(\theta_0 - \Delta\theta)] \sim f(\theta_0)\, \eta \ln \epsilon^{-1}. \tag{C 6}$$

(Here θ_0 is the static contact angle.) The result (C 6) may be anticipated by dimensional analysis, as it must be proportional to ηv^2, which then forces a logarithmic dependence on the slip scale cutoff. This gives rise to a contribution to the linear damping coefficient γ of the form

$$\gamma_1 = 4\omega \ln \epsilon^{-1} f(\theta_0)\, \kappa l^2 L^{-1}. \tag{C 7}$$

With the parameters of Tufillaro *et al.* (1989), $\theta_0 \sim \frac{1}{2}\pi$, and $s = 10$ Å, the ratio $\gamma_1/\gamma = 0.17$. This only gives an upper bound on the dissipation at the contact line, because we have not taken into account contact-angle hysteresis. Experimental systems typically have functions $\theta(v)$ with a discontinuity θ_h at $v = 0$ between a few and a few tens of degrees. If the amplitude of surface waves is small, so that the contact angle for a fixed meniscus is within θ_h of θ_0, the meniscus will not move, and no dissipation will occur at the contact line.

Finally, we consider the effect on dissipation of a layer of contamination (e.g. surface-active adsorbed molecules) at the free surface. Even if the two-dimensional viscosity of this two-dimensional liquid is neglected, the finite compressibility of the

layer changes the flow in such a way as to increase dissipation within l of the free surface. (The extreme case is an incompressible surface layer, which gives additional dissipation just as the side walls do.)

The situation has been analysed in detail by Miles (1967); we briefly summarize his results. The compressional stresses in the surface layer must be balanced by boundary-layer stresses resulting from some amount of slipping between the surface layer and the bulk over the skin depth l. That is, the stresses

$$\tau_s = i\omega^{-1} k^2 \chi(1-C)\, n, \quad \tau_v = \eta l^{-1} Cv \tag{C 8}$$

must balance. here v is the fluid velocity a distance l from the free surface; χ is the bulk modulus of the surface layer; and Cv is the relative velocity of the fluid and the surface layer.

Defining $\xi \equiv (\frac{1}{2}\eta\rho\omega^3)^{-\frac{1}{2}} k^2 \chi$ to be a characteristic ratio between viscous and compressive stresses, Miles finds $C = \xi/(\xi - 1 + i)$. Summing the viscous dissipation within the skin depth and the work done against the compressive stresses, the contribution γ_s to the damping coefficient is found to be

$$\gamma_s = \tfrac{1}{4}\omega k l \frac{\xi^2}{(\xi-1)^2+1}. \tag{C 9}$$

Note that γ_s is maximized for $\xi = 2$, which corresponds for the parameters of Tufillaro *et al.* (1989) to $\chi \sim 1.5\,\mathrm{erg\,cm^{-2}}$. (This modulus would also be evident as a reduction of the surface tension of a clean interface (Miles 1967); hence, a careful measurement of the dispersion relation can place a bound on how large a χ may be present.) The corresponding largest γ_s/γ ratio is about 2; hence a contaminated surface can lead to an observed γ three times the bulk contribution. For γ_s to be less than $\frac{1}{5}\gamma$, we require $\chi < 0.3\,\mathrm{erg\,cm^{-2}}$.

REFERENCES

Benjamin, T. B. & Ursell, F. 1954 *Proc. R. Soc. Lond.* A **225**, 505.

Bretherton, F. T. 1961 *J. Fluid Mech.* **10**, 166.

Ciliberto, S. & Gollub, J. 1985 *J. Fluid Mech.* **158**, 381.

Cox, R. G. 1986 *J. Fluid Mech.* **168**, 169.

Cross, M. C., Daniels, P. G., Hohenberg, P. C. & Siggia, E. D. 1983 *J. Fluid Mech.* **127**, 155.

Douady, S. & Fauve, S. 1988 *Europhys. Lett.* **6**, 221.

Eckhaus, W. 1965 *Studies in Non-linear Stability Theory*. Springer.

Ezerskii, A. B., Korotin, P. I. & Rabinovitch, M. I. 1985 *Pis'ma Zh. Eksp. Teor. Fiz.* **41**, 129.

Ezerskii, A. B., Rabinovitch, M. I., Reutov, V. P. & Starobinets, I. M. 1986 *Sov. Phys. J. Exp. Theor. Phys.* **64**, 1228.

Faraday, M. 1831 *Phil. Trans. R. Soc. Lond.* **121**, 319.

Hocking, L. M. 1987 *J. Fluid Mech.* **179**, 253.

Landau, L. D. & Lifshitz, E. M. 1959 *Fluid Mechanics*, p. 98. Pergamon.

Landau, L. D. & Lifshitz, E. M. 1976 *Mechanics* (3rd Edn), p. 80ff. Pergamon.

Levin, B. V. & Trubnikov, B. A. 1986 *Pis'ma Zh. Eksp. Teor. Fiz.* **44**, 311.

Miles, J. W. 1967 *Proc. R. Soc. Lond.* A **297**, 459.

Newell, A. C. & Whitehead, J. A. 1969 *J. Fluid Mech.* **38**, 279.

Riecke, H. 1990 Stable wave-number kinks in parametrically excited standing waves. ITP preprint, to be published.

Simonelli, F. & Gollub, J. P. 1989 *J. Fluid Mech.* **199**, 471.

Tufillaro, N. B., Ramshankar, R. & Gollub, J. P. 1989 *Phys. Rev. Lett.* **62**, 422.

Zakharov, V. E., L'vov, V. S. & Starobinets, S. S. 1971 *Sov. Phys., J. Exp. Theor. Phys.* **32**, 656.